BIOPHYSICS

Structure and sequence features of mussel adhesive protein lead to its salt-tolerant adhesion ability

Xinwen Ou[1]*, Bin Xue[2]*, Yichong Lao[1], Yanee Wutthinitikornkit[1], Ranran Tian[1], Aodong Zou[1], Lingyun Yang[3], Wei Wang[2], Yi Cao[2†], Jingyuan Li[1†]

Mussels can strongly adhere to hydrophilic minerals in sea habitats by secreting adhesive proteins. The adhesion ability of these proteins is often attributed to the presence of Dopa derived from posttranslational modification of Tyr, whereas the contribution of structural feature is overlooked. It remains largely unknown how adhesive proteins overcome the surface-bound water layer to establish underwater adhesion. Here, we use molecular dynamics simulations to probe the conformations of adhesive protein Pvfp-5β and its salt-tolerant underwater adhesion on superhydrophilic mica. Dopa and positively charged basic residues form pairs, in this intrinsically disordered protein, and these residue pairs can lead to firm surface binding. Our simulations further suggest that the unmodified Tyr shows similar functions on surface adhesion by forming pairing structure with a positively charged residue. We confirm the presence of these residue pairs and verify the strong binding ability of unmodified proteins using nuclear magnetic resonance spectroscopy and lap shear tests.

INTRODUCTION

Mussels can effectively adhere to the rocks in seawater by sequentially secreting various adhesive and cohesive proteins (*1*–*3*). Mussel adhesive proteins serve as the primer directly affecting mussel's ability to adhere to disparate material surfaces (*4*, *5*). The binding stability of adhesive proteins in salt solution has been well characterized over a wide spectrum of hydrophilic materials, e.g., layered silicates (*6*–*9*), metal oxides (*10*, *11*), and self-assembled monolayers (*12*). Protein adsorption needs to overcome a considerable barrier resulting from the stable hydration layer on hydrophilic materials (*13*–*15*). Moreover, the electrostatic screening effect of solution ions makes the establishment of strong adhesion even more difficult (*16*, *17*). Mussel adhesive proteins can address these challenges, enabling mussels to tenaciously attach to hydrophilic surfaces, despite that the molecular mechanism remains unclear.

A common feature of mussel adhesive proteins is the presence of the unusual amino acid Dopa (3,4-dihydroxy-L-phenylalanine; from posttranslational modification of Tyr) whose content ranges from 20 to 30 mol % (*6*, *15*). Previous study proposed that the adsorption of adhesive protein is through the direct interaction between Dopa and hydrophilic surface, e.g., the chelation with surface metal ions and the hydrogen bond with surface oxygens. However, the chelation interaction only occurs for a small fraction of metal (*18*) and metal oxides (*11*, *19*); the strength of hydrogen bond interaction of Dopa in aqueous environment is rather modest, not enough to explain the strong adhesion ability of adhesive protein (*20*, *21*). Besides, recent density functional theory (DFT) calculations suggested that Dopa only forms one hydrogen bond with hydrophilic phyllosilicates like mica (*22*) and saponite (*23*). On the other hand, there is substantial amount of Lys (10 to 20 mol %) in adhesive proteins (*24*, *25*). Growing evidence suggests that Lys also contributes to protein adhesion (*26*–*29*). In addition, the Dopa-based peptide containing insufficient Lys exhibits limited adhesion to hydrophilic surface (*30*). Moreover, increasing studies showed that the peptides containing Lys and unmodified Tyr can also adsorb to hydrophilic surfaces (*31*–*35*). Together, although the crucial role of Dopa to enhance the mussel attachment by promoting the protein cross-linking has been well established (*36*–*38*), its effect on adhesive interaction is under debate. Comprehensive understanding about the adhesive protein's binding ability is highly demanded, especially the mechanism about the contribution of these residues.

Molecular dynamics (MD) simulations have been widely used to study protein adsorption and the related structural feature (*39*–*41*). As for mussel adhesive proteins, their intrinsically disordered nature brings additional challenges to the simulation about their conformation and adsorption behavior. Previous computational studies on adhesive proteins mainly focused on the exploration of their solution conformations (*42*) and the optimization of the structure of preadsorbed protein fragments (*30*). Despite some effort (*43*), there is no computational work to describe the adsorption process of adhesive protein.

In this work, we combine MD simulation with nuclear magnetic resonance (NMR) spectroscopy and lap shear tests to study the conformational ensembles of adhesive protein Pvfp-5β and its adsorption behavior. The conformations of this intrinsically disordered protein are sampled by replica exchange MD (REMD) simulations. Dopa and positively charged basic residues (i.e., Lys and Arg) exhibit considerable spatial correlation and even form pair structure through cation-π interactions and hydrophobic matching. Moreover, such pair structure leads to the firm adhesion of protein on superhydrophilic mica. Dopa can reduce the stability of hydration layer, eliminate the hindrance caused by ions, and consequently facilitate the binding of its pairing basic residue. Hence, the pairing basic residue adheres to the negatively charged surface site by the electrostatic attraction, which contributes substantially to the binding stability of the proteins. The structure and binding ability of the

[1]Zhejiang Province Key Laboratory of Quantum Technology and Device, Institute of Quantitative Biology, Department of Physics, Zhejiang University, Zheda Road 38, Hangzhou 310027, China. [2]Collaborative Innovation Center of Advanced Microstructures, National Laboratory of Solid State Microstructure, Department of Physics, Nanjing University, Nanjing 210093, China. [3]iHuman Institute, Shanghai Tech University, 393 Hua Xia Zhong Road, Shanghai 201210, China.
*These authors contributed equally to this work.
†Corresponding author. Email: caoyi@nju.edu.cn (Y.C.); jingyuanli@zju.edu.cn (J.L.)

unmodified Pvfp-5β-Tyr are also studied. Strikingly, Tyr forms similar pair structure with positively charged basic residue. In addition, these residue pairs also lead to the firm adsorption of protein. Both spatial correlation and binding ability of Pvfp-5β-Tyr are further confirmed by NMR spectroscopy and lap shear tests, respectively. Our findings suggest that the pair structure of Tyr/Dopa with basic residues, rather than the posttranslational modification of Tyr to Dopa, should be responsible for the strong binding ability of mussel adhesive proteins.

RESULTS

The structure of Pvfp-5β in solution

We carry out REMD simulations to sample the conformational ensembles of intrinsically disordered Pvfp-5β. The cluster analyses (*44*) are then performed for the conformations of the 300-K replica, with a root mean square deviation cutoff of 3 Å. Representative configurations of the first six most populated clusters are then obtained (Fig. 1A and fig. S1). All these configurations share a prolate ellipsoidal shape with high content of random coils. The average solvent-accessible surface area and the radius of gyration (R_g) of protein are 67.67 nm^2 and 1.74 nm, respectively (fig. S2).

In these configurations, Dopa and positively charged basic residues tend to migrate to and stay on the protein surface. Dopa and basic residues exhibit considerable spatial correlation and can even form pairs. In our analysis, they are considered to pair up when the center of mass distance of their side chains is less than 5 Å. There are three Dopa-basic residue pairs in the most populated structure (Fig. 1, A to C). Such pair structure is commonly observed in the conformational ensembles we obtain. The average number of Dopa-basic residue pairs is 2.35. And the probability of at least two pairs is as high as 70%. In short, such unique pair structure is quite ubiquitous, although the mussel adhesive protein is intrinsically disordered.

The most populated conformation of the 300-K replica is adopted for the following 1000-ns simulation. The side chains of surface residues exhibit certain fluctuation, which is attributed to inherent thermal dynamics of protein and the interplay with the motion of hydration water (*45*). The root mean square fluctuations (RMSFs) are calculated to investigate the fluctuation of residues. Dopa residues (~2.49 Å) exhibit considerable fluctuation compared with non-Dopa residues (~1.34 Å). We further investigate the fluctuation of Dopa's aromatic ring by calculating the dihedral angles $\varphi_{C\text{-}CA\text{-}CB\text{-}CG}$ and $\varphi_{CA\text{-}CB\text{-}CG\text{-}CD1}$. Both dihedral angles undergo frequent fluctuation with the amplitude around 30°. In addition, the orientation of the aromatic ring even undergoes more marked transition with the amplitude of ~120° (fig. S3). Both results are in line with the previous simulation studies on the dynamics of Tyr aromatic ring (*46*–*48*).

The spatial correlation of all residue types is systematically analyzed by calculating the number of residues being in contact for each combination. And the contact matrix of adhesive protein is shown in Fig. 1D. The contact number for Dopa and Lys is considerably higher than for any other combinations. Asn exhibits certain spatial correlation with Dopa, while the tendency is weaker than Lys. We further calculate their radial distribution function (RDF; fig. S4): There is a main peak at r = 3.9 Å, corresponding to the direct contact between Dopa and Lys. It should be noted that the RDF of another positively charged basic residue Arg with respect to Dopa shares a similar trend (fig. S4). The modest contact number of Arg with Dopa is due to its much less occurrence (there are only three Arg residues). Therefore, both types of basic residue exhibit considerable spatial correlation with Dopa in this intrinsically disordered protein. The relative orientation of these pairing residues is analyzed by calculating the angle between their side chains (fig. S5C). The angle is mostly distributed in 0 to 30° (>80%), and more than 40% are within 10°: The side chains of the pairing Dopa and basic residues are largely parallel to each other.

Given by their parallel orientation, the hydrophobic carbonaceous groups of the side chains of pairing residues are largely overlapped, resulting in the hydrophobic matching effect (*49*, *50*). Moreover, the amino group of both Lys and Arg can establish the affinity with Dopa's aromatic ring (fig. S6) through cation-π interaction (*51*–*53*). Cation-π interaction is common in biological system (*54*–*56*). Previous studies also illustrated its prevalence in the peptides enriched with Lys and aromatic residues, which is considered to facilitate the interpeptide cross-linking and improve peptide adhesion (*31*, *32*). It should be noted that the hydrogen bond interaction between their side chains is rather weak (0.074 hydrogen

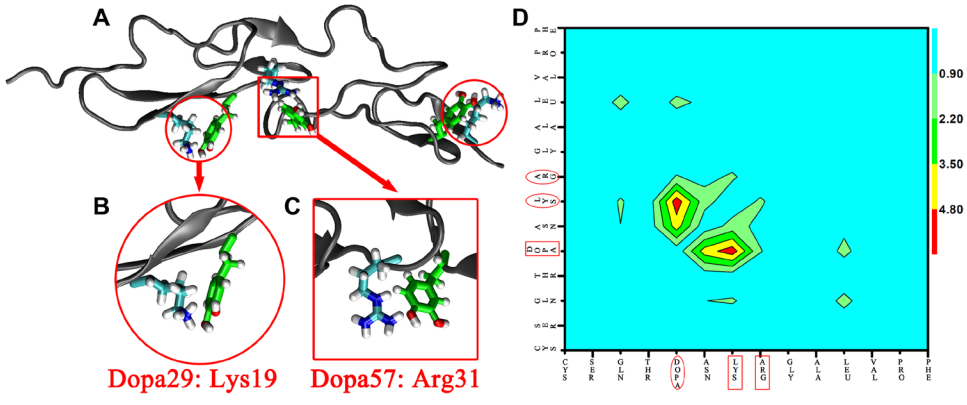

Fig. 1. Spatial correlation of basic residue and Dopa in mussel adhesive protein Pvfp-5β. (**A**) Typical configuration of protein Pvfp-5β, with three Dopa-basic residue pairs. (**B** and **C**) Pair structure of Dopa with Lys and Arg. Atoms are colored as follows: C (cyan), O (red), N (blue), and H (white); the C atoms of Dopa are shown in green. (**D**) Correlation matrix for all types of residues in protein, i.e., the average number of residues being in contact with other types of residues. Two residues are considered to be in contact if at least four pairs of heavy atoms are within 6 Å.

bond per residue pair) and has negligible contribution to the formation of residue pair. Together, this unique pair structure between Dopa and positively charged basic residue results from cation-π interaction and hydrophobic matching effect. Possible impact of the cations in solution to cation-π interaction between Lys and Dopa is further investigated in 150 mM NaCl solution. And cation has negligible interaction with Dopa, which does not affect the tendency of pair formation (fig. S7). Previous study also indicated that cation-π interactions within mussel protein remain unaffected in the condition of salt concentration at seawater level (>700 mM) (*57*). It should be noted that the stability of residue pairs is modest with an average lifetime of ~211 ps (fig. S5D), even though it is much stronger than the hydrogen bond involved by Dopa (with the lifetime of ~7 ps) (*58*). On the other hand, the formation of residue pairs is ubiquitous, which is largely due to the abundance of these residues (17 Dopa and 9 Lys, 3 Arg) and the structural flexibility of the intrinsically disordered adhesive protein. On a side note, in addition to the basic residues, the positively charged N terminus (N′) can also form pair with Dopa. In addition, the average number of these residue pairs in the 1000-ns trajectory is 2.75.

The adsorption of Pvfp-5β to mica

The adhesion ability of Pvfp-5β is then investigated by studying its adsorption to superhydrophilic mica. The protein is initially placed at least 10 Å away from the surface (Fig. 2A). Ten independent simulations are performed, and the protein can stably adsorb on mica in all trajectories (Fig. 2B and fig. S10).

As the adsorption proceeds, the number of contact atoms gradually increases (Fig. 2C). It should be noted that the growth of contact atoms is stepwise, and the adsorption process can roughly be represented in three steps. As shown in a representative trajectory, at t = 55 ns, the protein begins to contact with the surface, and the number of contact atoms increases to ~40 (step 1). At t = 126 ns, the number of contact atoms increases to ~120 (step 2). The number further increases to ~180 at t = 163 ns (step 3) and then remains constant. Representative snapshots of these steps are shown in fig. S8.

All these steps are triggered by the binding of Dopa-basic residue pairs and the pair formed by Dopa and N′ (Fig. 2D and movie S1). For example, the Dopa2-N′ pair binds to the surface, leading to the initial adsorption at t = 55 ns. Subsequently, the adsorption of middle part of protein (step 2) corresponds to the binding of Dopa29-Lys19 and Dopa57-Arg31 pairs. As for step 3, the adsorption of C-terminal part results from the binding of the Dopa70-Lys81 pair. The binding of these pairing residues facilitates the binding of the neighboring residues in all three steps (fig. S9). Similar stepwise adsorption can also be found in all other independent simulations (fig. S10). In simple terms, protein adsorption is dominated by Dopa-basic residue pairs.

A representative binding process of the Dopa-basic residue pair (i.e., Dopa29-Lys19) is chosen and studied in detail (Fig. 2E). We notice that the approaching residue pair is blocked by the stable hydration layer of superhydrophilic mica. The blocked Dopa keeps swinging, and the orientation of its side chain (the angle with respect to surface normal) fluctuates between 90° and 160° (fig. S11). The swinging Dopa enhances the diffusion of hydration water. The diffusion constant of water underneath the swinging Dopa is 1.47×10^{-5} cm^2/s (fig. S12), 2.3 times of the water diffusion underneath non-Dopa residue (0.65×10^{-5} cm^2/s; the paired positively charged residue is excluded). In addition, this diffusion rate is comparable to that on hydrophobic surfaces, e.g., graphene (*59*) and graphene-CH_3 (*60*). In other words, the side-chain swinging of Dopa blocked by the stable hydration layer can locally reduce the stability of hydration layer in return. Previous studies illustrated that the slowdown of hydration water of hydrophilic surfaces contributes to protein resistance, and the promotion of water diffusion is helpful to diminish the barrier formed by interfacial water and enhance protein adsorption (*13*, *14*).

We do observe that enhanced water diffusion and less stable hydration layer further facilitate the binding of pairing Lys19. As Dopa29 swings up at t = 125.9 ns, the neighboring water molecules are dragged away (Fig. 2E). Consequently, the underlying surface region is temporarily exposed. Thereafter, Lys19 protrudes through the hydration layer and binds to the surface driven by electrostatic attraction with the negatively charged surface site. The coupling between the swinging of Dopa29 and the binding of Lys19 in this interval (i.e., t = 125.90 to 125.96 ns) is then estimated by the cross-correlation function, $C(\tau) = \frac{\langle z(t) \cdot \theta(t-\tau) \rangle}{\langle z(t) \cdot \theta(t) \rangle}$, where z and θ are the position of Lys amino group and the orientation of Dopa, respectively, and τ refers to the time delay of correlation (fig. S13). The maximum of the cross-correlation function is observed at τ = 34 ps, only one-seventh of the lifetime of the residue pair (211 ps). In short, the behaviors of the pairing Dopa29 and Lys19 are highly correlated, facilitating Lys protrusion through the stable hydration layer of mica. Similar phenomenon can be found for the binding of other residue pairs (fig. S14). During the approaching process, the fluctuation amplitude of Dopa's side chain (with the RMSF of 2.39 Å) is similar to the case in solution. In addition, the RMSF of non-Dopa is 1.43 Å. These residues also exhibit certain inherent fluctuations with the amplitude weaker than Dopa.

When both residues adsorb to mica, the interaction energy of Lys19 with mica is much stronger than that of Dopa29 (−280.56 versus −5.42 kJ/mol; fig. S15) and is comparable to the coordination interaction in protein adhesion (*18*, *19*). The similar phenomenon is also observed for other residue pairs. The binding affinity of protein should be attributed to the electrostatic attraction of positively charged basic residue with the surface, rather than the hydrogen bond formed by contacted Dopa (the number of hydrogen bonds per adsorbed Dopa is only 0.41; fig. S16). Previous MD simulation also suggests that Dopa forms at most one hydrogen bond with the surface (*61*). Dopa intermittently forms one hydrogen bond with polydimethylsiloxane, and the probability of hydrogen bonding is well below 50%. We also calculate the energy of hydrogen bond between Dopa and mica, and the average energy is −25.2 kJ/mol, which is close to the DFT calculations: The hydrogen bond energies of Dopa with hydrophilic phyllosilicates such as mica and saponite are −27.9 kJ/mol (*22*) and −28.9 kJ/mol (*23*), respectively. Together, the interaction of Dopa with mica is much weaker than that of Lys (fig. S17). Our findings are in agreement with previous experiments: The interaction of contacting Dopa with mica and other hydrophilic surfaces is limited (*20*, *21*). In other words, Dopa acts as a catalyst to reduce the stability of hydration layer of the hydrophilic surface.

We investigate the adsorption of the adhesive protein in the salt solution (150 mM NaCl). As described above, protein adsorption is attributed to the electrostatic attraction with mica. In salt solution, this attraction is attenuated by the electrostatic screening effects of ions: The cations can adsorb to the surface sites, while the anions tend to bind to the positively charged basic residues (fig. S18). The adhesive protein can effectively adsorb on superhydrophilic mica in

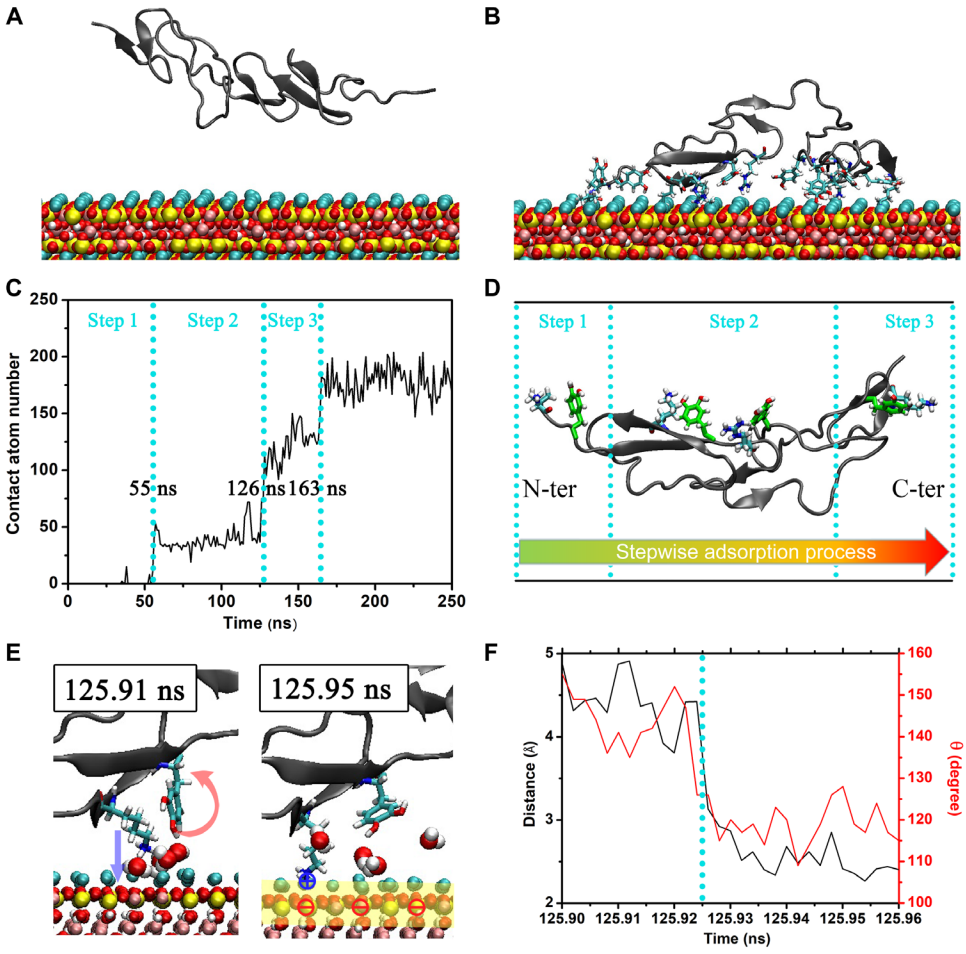

Fig. 2. Protein adsorption on mica. (**A** and **B**) Initial and final configurations of the protein adsorption. The atoms of mica are colored as follows: Si (yellow), Al (pink), K (cyan), O (red), and H (white). (**C**) Number of contact atoms of protein. (**D**) Residue pairs participating in the protein adsorption. (**E**) Representative snapshots of the binding of the Dopa29-Lys19 pair. (**F**) Distance between the NH_3^+ of Lys19 and mica surface (black line) and the angle between the aromatic ring of Dopa29 and surface normal of mica (red line).

a stepwise manner (Fig. 3 and fig. S19). In addition, this stepwise adsorption is also triggered by the binding of residue pairs. Moreover, the number of contact atoms in 150 mM NaCl solution (~153) is comparable to that in water (~179; both are based on the last 50-ns trajectory). The interaction energies between protein and surface in both cases are also similar: −1390 and −1265 kJ/mol for water and 150 mM NaCl solution, respectively (fig. S17).

During the adsorption of the residue pair, the behaviors of Dopa and basic residue also exhibit considerable correlation, which further reduce the adverse impacts of ions on adhesion (Fig. 3, C and D). For example, during the binding of the Dopa29-Lys19 pair at $t \sim 443$ ns, one Cl^- in the hydration layer is initially bound to Lys19 from below. The swinging Dopa29 drags the water molecules away from the hydration layer, and Lys19 then tilts downward to the temporally exposed region and eludes the bound Cl^-. During the adsorption of the Dopa70-Lys81 pair (at $t \sim 831$ ns), one K^+ initially occupies the negatively charged surface site and blocks the binding of Lys81. Water diffusion enhanced by the swinging Dopa70 can further trigger the movement of K^+ (fig. S20, C and D). Similar phenomena of the exclusion of cations can also be found in the binding process of the Dopa3-N′ pair (fig. S20, A and B). It should be noted that the surface ions on mica are hydrated. During these eviction processes, the cations all keep hydrated (fig. S21). In short, the swinging of Dopa reduces the screening effect of ions and facilitates the binding of its pairing basic residue. We also study the protein adsorption at even higher salt concentration (i.e., 300 mM NaCl). The protein can still overcome the impact of ions and effectively adsorb to mica (fig. S22).

The structure and adsorption of the unmodified protein Pvfp-5β-Tyr

As mentioned above, Dopa and positively charged basic residues exhibit considerable spatial correlation within Pvfp-5β and even form pairing structure. This correlation is attributed to the cation-π interaction and hydrophobic matching and does not involve the extra hydroxyl group of Dopa. The subsequent protein adsorption is then based on the coupling between the swinging of Dopa and the protrusion of basic residue without the contribution from the catechol group. Thus, we hypothesize that the unmodified protein, namely, Pvfp-5β-Tyr, may also exhibit considerable surface binding if the Tyr-basic residue pairs exist. The conformational ensembles of Pvfp-5β-Tyr are first investigated (Fig. 4). Tyr also exhibits considerable spatial correlation with basic residues. For example, the

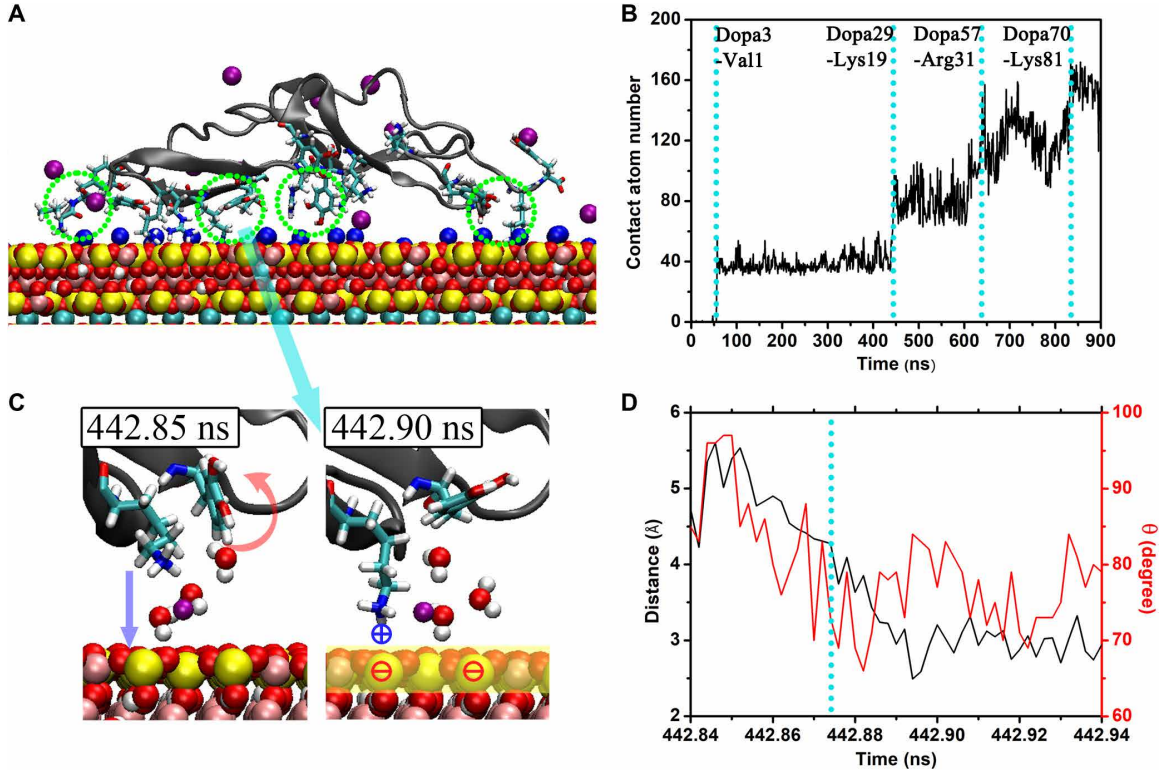

Fig. 3. Protein adsorption on mica in 150 mM NaCl solution. (**A**) Typical configuration of the protein adsorbed on mica. The residue pairs are denoted by green dotted circles. Na^+ is shown in blue; Cl^- is shown in purple; K^+ and water are not shown for clarity. (**B**) Number of contact atoms of protein. (**C**) Representative snapshots of the binding of the Dopa29-Lys19 pair. (**D**) Distance between the NH_3^+ of Lys19 and mica surface (black line) and the angle between the aromatic ring of Dopa29 and surface normal of mica (red line).

average contacting residue of Tyr with Lys is 5.20 and is comparable to Pvfp-5β (5.59 residues). Such correlation also leads to the formation of Tyr-basic residue pairs. And the average number of residue pairs (2.73) is also close to the case of Pvfp-5β (2.35 pairs). In addition, Tyr's RMSF (~2.22 Å) is also considerably higher than non-Tyr residues (~1.37 Å). In other words, the difference of one aromatic hydroxyl group does not affect the thermal fluctuation of Tyr and its spatial correlation with positively charged basic residues.

In addition, we perform five independent simulations to study the protein adsorption on mica, and the protein can stably adsorb on mica in all trajectories (Fig. 4 and fig. S23). The number of contact atoms with mica is ~170, comparable with that of Pvfp-5β (~179). Similarly, the adsorption process is stepwise, triggered by the binding of the Tyr-basic residue pair. The behaviors of Tyr and basic residue are highly coupled during their adsorption. For example, swinging Tyr29 drags the water molecules away from the hydration layer that facilitates the binding of the pairing Lys19 to the mica surface (t = 87.4 ns; fig. S24). Such correlation can be found in the binding process of other residue pairs (e.g., Tyr2-N′ and Tyr70-Lys81; fig. S25). Moreover, the protein can also bind to mica in 150 mM NaCl solution (fig. S26). The number of contact atoms in water and 150 mM NaCl solution is also comparable (170 versus 171, based on the last 50-ns trajectory). In addition, Pvfp-5β-Tyr shows comparable adsorption stability in both systems (−1192 kJ/mol in water versus −1208 kJ/mol in 150 mM NaCl solution; fig. S17). Thus, the swinging of Tyr can also reduce the screening effect of ions and facilitate protein adsorption. This finding provides a mechanistic explanation of intriguing experimental studies of the binding of Tyr-containing biomimetic peptides (*31*, *32*). It has been found that these peptides can strongly bind to mica in 250 mM NaCl solution without Dopa modification (*31*).

Experimental verification

The spatial correlation between Lys and Tyr of the unmodified adhesive protein is verified by liquid-state NMR spectroscopy. Two-dimensional (2D) ^1H-^{13}C heteronuclear single-quantum coherence (HSQC) experiment is used for the assignment of the ^1H directly bonded to the ^{13}C of Lys of the peptide derived from Pvfp-5β-Tyr. In addition, the ^1H signals at 1.5 to 1.9 ppm can be assigned to the alkyl group (R-CH_2-R) of Lys (fig. S27). The 2D ^1H-^1H nuclear Overhauser effect spectroscopy (NOESY) is then used to investigate the correlation between the ^1H nuclei (Fig. 5A). Although the spectroscopy mainly includes the intensity correlations that result from intra-residue interactions, there is well-defined correlation corresponding to the dipolar coupling of ^1H nuclei of Lys and Tyr. More specifically, the ^1H signals at 1.5 to 1.9 ppm of the alkyl group of Lys are correlated with ^1H signals at 6.9 to 7.1 ppm of the aromatic hydrogen atoms of Tyr. This correlation indicates the close proximity of the side chains of Tyr and Lys. Our results are consistent with previous NMR study that also suggests the proximity of Tyr and Lys and the formation of cation-π interaction in the synthetic adhesive peptides (*31*).

The adhesion of the unmodified protein Pvfp-5β-Tyr on hydrophilic materials is evaluated using lap shear tests. The adhesion

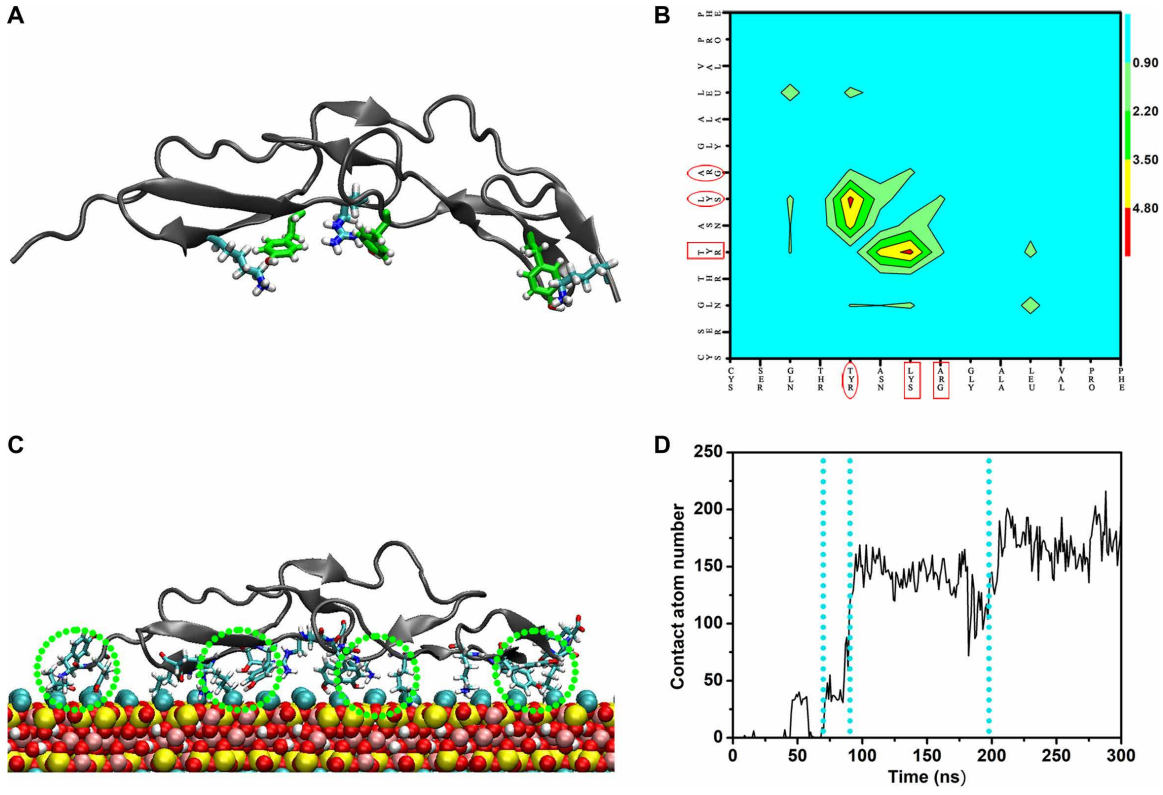

Fig. 4. Conformation and adsorption of the unmodified protein Pvfp-5β-Tyr. (**A**) Typical configuration of Pvfp-5β-Tyr, with three Tyr-basic residue pairs. (**B**) Correlation matrix for all types of amino acids in protein. (**C**) Representative configuration of the protein adsorbed on mica. The residue pairs are denoted by green dotted circles. (**D**) Number of contact atoms of protein.

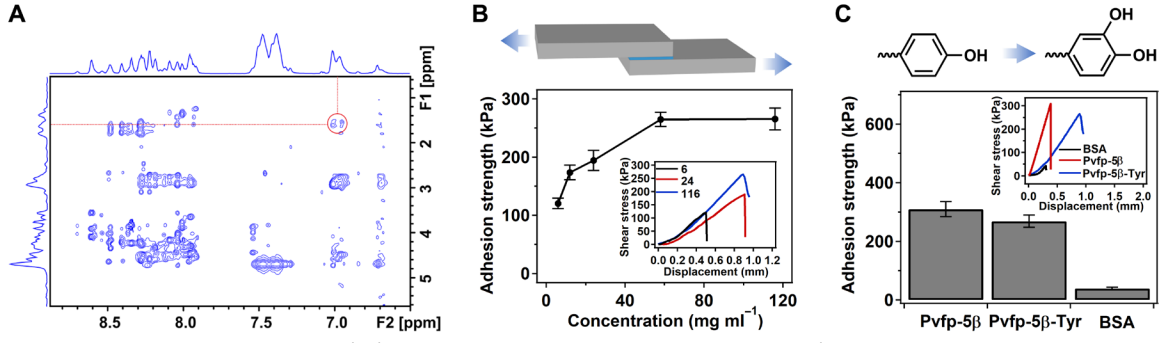

Fig. 5. NMR spectroscopy and lap shear tests. (**A**) 2D ^{1}H-^{1}H NOESY NMR spectrum of the peptide with the 1D ^{1}H NMR spectrum along the top horizontal axis and the left vertical axis. The red circle indicates the correlated intensity that results from the close proximities of the aromatic hydrogen of Tyr and the alkyl hydrogen of R-CH_2-R of Lys. (**B**) Schematic of lap shear measurements of the unmodified protein Pvfp-5β-Tyr (buffer: 150 mM NaCl solution) and the summarized adhesion strength at varied protein concentrations. The inset is the typical stress-extension curves of lap shear measurements at the protein concentrations of 6, 24, and 116 mg ml^{-1} after curing for 16 hours in air. (**C**) Schematic of conversion from Pvfp-5β-Tyr to Pvfp-5β and the summarized adhesion strength of BSA, Pvfp-5β-Tyr, and Pvfp-5β at the protein concentration of 116 mg ml^{-1} (buffer: 150 mM NaCl solution) after curing for 16 hours in air. The inset is the typical stress-extension curves of lap shear measurements for three proteins.

strength is determined by the maximum force that separates the overlapped glass slides bonded by the proteins. The adhesion of proteins of different concentrations (6 to 116 mg ml^{-1} dissolved in ddH_2O or 150 mM NaCl solution) is investigated separately (Fig. 5B and fig. S28). The samples are cured for 16 hours in air before the lap shear test. We find that the adhesion strength is gradually increased as the curing proceeds (fig. S29), which may be due to the loss of water and the enhancement of the cohesion among Pvfp-5β-Tyr chains during the curing process. However, the protein solution sandwiched between two substrates is not fully dried out, and the water content of the protein solution remains to be ~50% after 16-hour curing (fig. S30). For these as-prepared samples, they all exhibit strong adhesion. Even at the lowest protein concentration (6 mg ml^{-1} in 150 mM NaCl solution), the adhesion strength

can be as high as 120 kPa, which is stronger than the shear strength of many mussel-mimetic adhesives on glass (*29*, *62*–*65*). The adhesion strength further increases to 265 kPa (116 mg ml^{-1}) as the protein concentration increases (Fig. 5B and fig. S28). In sharp contrast, the adhesion strength of a commonly used nonadhesive protein, bovine serum albumin (BSA), is as low as 40 kPa under the same conditions (Fig. 5C). Furthermore, we perform the lap shear experiments using the modified protein Pvfp-5β (i.e., the polyphenol oxidase–treated protein) to reveal the contribution of posttranslational modification of Tyr to Dopa to adhesion. As shown in Fig. 5C and fig. S31, the adhesion strengths of Pvfp-5β and Pvfp-5β-Tyr are similar when the curing time is relatively short. The adhesion strength of Pvfp-5β-Tyr reaches a plateau of ~265 kPa after curing for 12 hours. The adhesion strength of Pvfp-5β with similar curing time (16 hours) is ~310 kPa, while it keeps increasing even after 36 hours of curing. The steady increase of the adhesion strength may result from the oxidation of Dopa, which strengthens intermolecular interactions and prevents cohesion failure in the lap shear tests. It is worth mentioning that the adhesion ability of the protein tested in ddH_2O or salt solutions is similar to that in air (fig. S32), which also suggests that the adhesion stability does not simply result from the protein dehydration during the curing process.

Moreover, we perform the underwater adhesion experiments in either water (i.e., ddH_2O) or ionic (i.e., 150 mM NaCl) environments (fig. S33). Pvfp-5β-Tyr solution can effectively join two glass slides under water. Because of the inevitable diffusion of protein during the adhesion operation, the adhesion strength of Pvfp-5β-Tyr in aqueous environment is somewhat lower than that in air but still reaches 150 kPa in ddH_2O and 118 kPa in 150 mM NaCl solution, respectively (fig. S33C). In contrast, BSA solution cannot even join two glass slides under water. We notice that Pvfp-5β-Tyr can form coacervated phase in ddH_2O or 150 mM NaCl solution (fig. S33, D and E). This liquid-liquid phase-separation behavior slows down the diffusion of proteins to aqueous environment during the adhesion operation and therefore ensures strong underwater adhesion.

To reveal the adhesion failure mechanism, we investigate the surface of the glass slides using both atomic force microscopy (AFM) imaging and protein staining. As shown in fig. S34, the height of the interlayer is about 50 to 110 nm for both the adhesion in ddH_2O and in 150 mM NaCl solution. Moreover, the protein spreads on both the A and B sides of the glass after the failure according to the protein staining experiments using InstantBlue (fig. S35). Both AFM and microscopic images show that proteins are sporadically distributed on both surfaces, suggesting a combined cohesion and adhesion failure (*29*).

The adhesion of Pvfp-5β-Tyr solution on other substrates in addition to glass [i.e., SiO_2, Si, poly(methyl methacrylate) (PMMA), and Fe] is also studied. The adhesion strengths for SiO_2 and Si substrates are also higher than 200 kPa, much higher than that for the PMMA and Fe substrates (fig. S36). The much weaker adhesion strength for PMMA and Fe substrates suggests that the electrostatic interaction plays an important role in the protein adhesion because the surfaces of PMMA and Fe substrates are not negatively charged.

Together, the adhesion strength of the unmodified protein Pvfp-5β-Tyr in the absence of protein-protein cross-linking mediated by Dopa (i.e., 265 kPa for glass) is already comparable to the tensile strength of mussel byssal threads (measured by pulling them apart from glass, 171 to 310 kPa) (*66*). Our results show that the unmodified protein Pvfp-5β-Tyr has very strong ability to bind to the hydrophilic surface. Moreover, the comparison with the adhesion strength of Pvfp-5β suggests that the superior adhesion ability of mussel adhesive protein may be irrelevant to the posttranslational modification of Tyr to Dopa.

DISCUSSION

In this work, we reveal a considerable spatial correlation between Dopa and positively charged basic residues (i.e., Lys and Arg) of intrinsically disordered protein Pvfp-5β. Similar spatial correlation between Tyr and basic residues can be found in the unmodified counterpart Pvfp-5β-Tyr. Both Dopa and Tyr can form pairs with positively charged basic residue through cation-π interaction and hydrophobic matching effect. The existence of these residue pairs leads to the firm adhesion of the protein on superhydrophilic mica. The aromatic residues (Dopa and Tyr) swing back and forth, thereby scattering interfacial water molecules and eliminating the electrostatic screening effect of surface ions. The pairing basic residue then protrudes and binds to the negatively charged site on the surface. While the binding stability of the protein is largely attributed to the electrostatic attraction of the positively charged basic residue to the negatively charged surface site, the aromatic residue essentially supports the protein adsorption by paving the way for the basic residue to approach the mica surface. Thus, the salt-tolerant underwater adhesion of the adhesive protein can be attributed to the residue pair within this flexible macromolecule.

As indicated in a recent work about mussel-mimic peptide and the ones with Dopa replaced by Tyr and Phe (*31*), cation-π interaction occurs in all these three peptides: Lys and aromatic residues tend to form cation-π interactions in the peptides enriched with these two types of residues. Besides, a recent work on the adsorption behavior of copolymer also found that aromatic residues enhance electrostatic interaction of their adjacent cationic residues with the surface (*67*). In addition, as a small amount of Dopa or Tyr (~10%) is conjugated to poly-lysine, its adsorption ability is enhanced to a similar extent (*28*, *68*). Further increase of Dopa content cannot improve the adsorption ability of this polymer, which suggests that the contribution of these aromatic residues in the direct binding with surface may be very limited. Another study of Dopa-containing polymer also found a rather modest hydrogen bond interaction with mica (*20*). In our previous work on polyethylene glycol–conjugated dipeptides, the adhesion ability of Lys-Dopa dipeptides is much stronger than Gly-Dopa, suggesting that Lys residue contributes to the surface binding. Besides, the adhesion ability of dipeptides with Lys at the N terminus (Lys-Dopa) is stronger than C terminus (Dopa-Lys), indicating that the cooperative Lys and Dopa binding to hydrophilic surfaces strongly depends on the protein sequences (*29*). As for the adhesive proteins, increasing studies also showed that recombinant protein enriched with Tyr rather than Dopa has strong adhesive ability (*32*–*35*). All these studies are consistent with our findings based on MD simulations and lap shear experiments. In other words, the pairing structure and the realization of adsorption ability may also appear in these adhesive proteins. On the other hand, the adsorption behavior of catechol-containing small molecules (*26*) is distinct from adhesive protein macromolecules or biomimetic polymers. It is difficult for small molecules to realize stable adhesion in the form of monomer, and their adhesion relies on film formation by cross-linking. Hence, in addition to the direct binding with the surface, the adhesion ability of small molecule is dependent on the

intermolecular cross-linking. And Dopa's catechol group can promote this cross-linking (e.g., hydrogen bonding and Michael addition), thereby facilitating adhesion.

We conclude that the pair structure that emerges in the adhesive protein, rather than modification of Tyr to Dopa, should be crucial to its extraordinary salt-tolerant adhesion ability. Our findings highlight the importance of sequence and structure features of adhesive protein: The occurrence of the residue pair is largely due to the abundance of cationic and aromatic residues and the structural flexibility of the protein. These features and the resulting spatial correlation between two types of residues should be taken into account to improve the adhesion performance of mussel-mimetic materials.

MATERIALS AND METHODS

The structure of protein in solution

The unmodified protein Pvfp-5β consists of 82 residues, including 17 Tyr (Y) and 9 Lys (K), and the sequence is VYYPNPCSPYPCRNGGTCKKRGLYSYKCYCRKGYTGKNCQYNACFPNPCLNGGTCGYVYGYPYYKCSCPYGYYGKQCQLKKY (*4*, *42*). The structure of unmodified Pvfp-5β is built using standard homology modeling techniques following a previous study (*42*). The DEL-1 epidermal growth factor (EGF) domain [Protein Data Bank ID: 4D90 (*69*)] is chosen as the structural template, which has 51% sequence identity homologous to unmodified Pvfp-5β. Ten possible models are constructed using the Modeller software (*70*), and the one with the lowest discrete optimized protein energy score (*71*) is selected (denoted as Pvfp-5β-Tyr). Then, all Tyr residues are modified to Dopa to obtain the model of Pvfp-5β.

Two series of REMD simulations (*72*) are then performed to probe the conformational space of both Pvfp-5β and Pvfp-5β-Tyr. For each series, 86 replicas are used with temperatures ranging from 300 to 420 K. The temperatures of the replicas are determined by the method proposed by Patriksson and van der Spoel (*73*). The exchange between neighbor replica is attempted every 1 ps, and the average exchange probability is ~22%. The replicas run in parallel for 50 ns, and the total simulation time of REMD of each series is 4.3 μs. The most popular conformation of the 300-K replica of both Pvfp-5β and Pvfp-5β-Tyr is adopted to perform a 1-μs *NPT* ensemble simulation (300 K and 1 atm), which is used to analyze the solution structure of protein, especially the lifetime of the residue pair.

The adsorption of protein to mica

Mica (monoclinic, C2/c symmetry), with chemical formula $KAl_2(Si_3Al)O_{10}(OH)_2$, has a TOT (tetrahedral-octahedral-tetrahedral) layer structure. Because of partial substitution of tetrahedral Si by Al, the tetrahedral layer has a net negative charge, which is neutralized by the naturally adsorbed K^+ ions. In this study, the lattice constants of mica are taken from high-resolution x-ray reflectivity (*74*), and the tetrahedral Al atoms are arranged following the Loewenstein's rule (*75*). The mica substrate consists of a 20a × 12b × 1c crystallographic unit cell and cleaved by the (001) plane, and half of the K^+ ions remain on the surface.

The protein is initially placed at least 10 Å above the mica surface. The system is solvated in a water box (~30,000 water molecules) with the size of 10.36 nm × 10.74 nm × 10.62 nm. Because Pvfp-5β is positively charged, 12 Cl^- counterions are added to neutralize the system. Ten independent simulations are performed, and the protein can stably adsorb on mica in all trajectories (Fig. 2 and fig. S10). We also perform five independent simulations to study the protein adsorption in 150 mM NaCl solution. In these simulations, protein can also bind to mica, and the results are shown in Fig. 3 and fig. S19. The adsorption of the unmodified protein Pvfp-5β-Tyr on mica in water and 150 mM NaCl solution is also investigated, and the protein can also firmly adsorb on mica in both cases. The results are shown in Fig. 4 and figs. S23 to S25. All simulations are performed in *NPT* ensemble at 300 K and 1 atm.

Computational details

The system temperatures are controlled using the velocity-rescaled Berendsen thermostat (*76*). The isotropic Berendsen pressure coupling is used for the simulation of protein in water, and the semi-isotropic Berendsen pressure coupling is used for the simulation of protein adsorption (*77*). The interaction of mica is described by the CLAYFF force field (*78*). The potential parameters for protein are taken from the CHARMM36 force field (*79*), and the parameters of Dopa are obtained from the CHARMM General Force Field (table S1) (*80*, *81*). For water molecule, the TIP3P model is chosen (*82*). The periodic boundary conditions are applied in all directions (*83*). A typical 1.2-nm cutoff distance is used to calculate the short-range electrostatic interaction and the van der Waals interaction. The particle mesh Ewald method is used to compute the long-range electrostatic interaction (*84*). The LINCS algorithm is adopted to constrain the bond vibrations involving hydrogen atoms (*85*), allowing a time step of 2 fs. All the MD simulations are carried out using the GROMACS 5.1.2 package (*86*), and snapshots are rendered by the visual molecular dynamics (VMD) program (*87*).

Protein synthesis

The gene encoding protein Pvfp-5β-Tyr is constructed in pET30a vectors using standard molecular biology techniques, and the plasmid is purchased from GenScript (Nanjing, China). The protein fused with His-SUMO tag is expressed in *Escherichia coli* (BL21), purified by Co^{2+} affinity chromatography, and identified by SDS–polyacrylamide gel electrophoresis and circular dichroism spectra (fig. S37). The protein is dialyzed into deionized water and lyophilized before lap shear measurements.

In addition, the 25–amino acid peptide (sequence: KKRGLYSYKCYCRKGYTGKNCQYNA) derived from Pvfp-5β-Tyr is commercially synthesized using solid-phase peptide synthesis (GL Biochem, Shanghai, China), where the Lys (K) is enriched with ^{13}C. The peptide is detected by high-performance liquid chromatography and mass spectrometry analysis. The peptide is then used to study the spatial correlation between Lys and Tyr by liquid-state NMR spectroscopy.

NMR spectroscopy

NMR spectra of protein samples with 90% H_2O/10% D_2O are measured with a Bruker 800M Hz AVANCE III spectrometer at 25°C, using a ^1H-^{13}C-^{15}N triple resonance probe. The 1D ^1H NMR spectra are recorded with 32k complex points, which are zero-filled to 64k points; the relaxation delay is 2 s. The 2D ^1H-^1H NOESY spectra are recorded with 2k and 256 complex points in the direct and indirect dimension, respectively. The mixing time is 120 ms. The 2D ^1H-^{13}C HSQC spectra are recorded with 2k and 256 complex points in the direct and indirect dimension, respectively. The line-broadening factor of the QSINE function is 1 Hz.

Lap shear measurements

In the lap shear experiments, hydrophilic glass surfaces, instead of mica surfaces, are used because shearing mica surfaces glued by the adhesive proteins often results in the peel off of mica layers, and the results do not reflect the real adhesion strength between the protein and the surface. The hydrophilic glass surfaces are prepared as follows: The glass slides are immersed into the chromic acid solution for about 12 hours at room temperature and cleaned with ddH_2O. These glass substrates are used directly or further amino-functionalized using 10% (w/v) (3-aminopropyl) triethoxysilane in toluene and extensively washed by ethanol and ddH_2O to make the surface superhydrophilic. The two cleaning approaches do not cause any measurable differences on the adhesion strength. All the glass substrates are stored at 4°C before use.

To measure the adhesion strength, the glass substrates are adhered with proteins in either ddH_2O or 150 mM NaCl solution. The protein concentrations are fixed at 116 mg ml^{-1} unless otherwise specified. The width and length of the adhesion areas are about 10.0 and 8.0 mm, respectively. About 20 μl of protein solutions is applied on the top of substrates, and the adhered substrates are fixed with a clamp in preparing each sample. The curing of the adhesion is conducted in air for 16 hours unless otherwise specified. All the lap shear tests are performed with a mechanical testing machine (Instron-5944 with a 2 kN sensor) in either air, ddH_2O, or 150 mM NaCl solution at room temperature, and the tensile speed is kept at 10 mm min^{-1}. Shear strength is determined by dividing the maximum force by the adhesion area. The same method described above is also used for the lap shear experiments of other kinds of substrates.

To prepare the Pvfp-5β sample, Pvfp-5β-Tyr and the polyphenol oxidase (NJDULY, Nanjing, China) are dissolved into phosphate-buffered saline solution (10 mM; pH 7.4) at the molar ratio of 10:1 and incubated at 37°C for 24 hours under the protection of argon. Then, the solution is centrifuged at 8000 rpm for 30 min for three times with ultrafiltration (30k, Amicon Ultra-4, Millipore, USA) to separate Pvfp-5β and polyphenol oxidase. The obtained Pvfp-5β solution is dialyzed and lyophilized before the lap shear measurements.

SUPPLEMENTARY MATERIALS

Supplementary material for this article is available at http://advances.sciencemag.org/cgi/content/full/6/39/eabb7620/DC1

View/request a protocol for this paper from *Bio-protocol*.

REFERENCES AND NOTES

1. J. H. Waite, M. L. Tanzer, Polyphenolic substance of *Mytilus edulis*: Novel adhesive containing L-DOPA and hydroxyproline. *Science* **212**, 1038–1040 (1981).
2. R. J. Stewart, T. C. Ransom, V. Hlady, Natural underwater adhesives. *J. Polym. Sci. B Polym. Phys.* **49**, 757–771 (2011).
3. L. Petrone, Molecular surface chemistry in marine bioadhesion. *Adv. Colloid Interface Sci.* **195-196**, 1–18 (2013).
4. P. A. Guerette, S. Hoon, Y. Seow, M. Raida, A. Masic, F. T. Wong, V. H. Ho, K. W. Kong, M. C. Demirel, A. Pena-Francesch, S. Amini, G. Z. Tay, D. Ding, A. Miserez, Accelerating the design of biomimetic materials by integrating RNA-seq with proteomics and materials science. *Nat. Biotechnol.* **31**, 908–915 (2013).
5. D. S. Hwang, H. Zeng, A. Masic, M. J. Harrington, J. N. Israelachvili, J. H. Waite, Protein- and metal-dependent interactions of a prominent protein in mussel adhesive plaques. *J. Biol. Chem.* **285**, 25850–25858 (2010).
6. Q. Lin, D. Gourdon, C. Sun, N. Holten-Andersen, T. H. Anderson, J. H. Waite, J. N. Israelachvili, Adhesion mechanisms of the mussel foot proteins mfp-1 and mfp-3. *Proc. Natl. Acad. Sci. U.S.A.* **104**, 3782–3786 (2007).
7. A. H. Hofman, I. A. van Hees, J. Yang, M. Kamperman, Bioinspired underwater adhesives by using the supramolecular toolbox. *Adv. Mater.* **30**, e1704640 (2018).
8. Q. Lu, E. Danner, J. H. Waite, J. N. Israelachvili, H. Zeng, D. S. Hwang, Adhesion of mussel foot proteins to different substrate surfaces. *J. R. Soc. Interface* **10**, 20120759 (2013).
9. M. Cui, S. Ren, S. Wei, C. Sun, C. Zhong, Natural and bio-inspired underwater adhesives: Current progress and new perspectives. *APL Mater.* **5**, 116102 (2017).
10. C. Fant, K. Sott, H. Elwing, F. Hook, Adsorption behavior and enzymatically or chemically induced cross-linking of a mussel adhesive protein. *Biofouling* **16**, 119–132 (2000).
11. J. Yu, W. Wei, M. S. Menyo, A. Masic, J. H. Waite, J. N. Israelachvili, Adhesion of mussel foot protein-3 to TiO_2 surfaces: The effect of pH. *Biomacromolecules* **14**, 1072–1077 (2013).
12. J. Yu, Y. Kan, M. Rapp, E. Danner, W. Wei, S. Das, D. R. Miller, Y. Chen, J. H. Waite, J. N. Israelachvili, Adaptive hydrophobic and hydrophilic interactions of mussel foot proteins with organic thin films. *Proc. Natl. Acad. Sci. U.S.A.* **110**, 15680–15685 (2013).
13. Y. He, Y. Chang, J. C. Hower, J. Zheng, S. Chen, S. Jiang, Origin of repulsive force and structure/dynamics of interfacial water in OEG–protein interactions: A molecular simulation study. *Phys. Chem. Chem. Phys.* **10**, 5539–5544 (2008).
14. J. Zheng, L. Li, H.-K. Tsao, Y.-J. Sheng, S. Chen, S. Jiang, Strong repulsive forces between protein and oligo (ethylene glycol) self-assembled monolayers: A molecular simulation study. *Biophys. J.* **89**, 158–166 (2005).
15. B. P. Lee, P. B. Messersmith, J. N. Israelachvili, J. H. Waite, Mussel-inspired adhesives and coatings. *Annu. Rev. Mater. Res.* **41**, 99–132 (2011).
16. J. Buijs, V. Hlady, Adsorption kinetics, conformation, and mobility of the growth hormone and lysozyme on solid surfaces, studied with TIRF. *J. Colloid Interface Sci.* **190**, 171–181 (1997).
17. M. Lundin, U. M. Elofsson, E. Blomberg, M. W. Rutland, Adsorption of lysozyme, β-casein and their layer-by-layer formation on hydrophilic surfaces: Effect of ionic strength. *Colloids Surf. B. Biointerfaces* **77**, 1–11 (2010).
18. T. Chen, H. Yang, H. Gao, M. Fu, S. Huang, W. Zhang, G. Hu, F. Liu, A. Ma, K. Sun, J. Wang, Adsorption and orientation of 3,4-dihydroxy-L-phenylalanine onto tunable monolayer films. *J. Phys. Chem. C* **121**, 11544–11551 (2017).
19. M. Vega-Arroyo, P. R. LeBreton, T. Rajh, P. Zapol, L. A. Curtiss, Density functional study of the TiO_2–dopamine complex. *Chem. Phys. Lett.* **406**, 306–311 (2005).
20. T. H. Anderson, J. Yu, A. Estrada, M. U. Hammer, J. H. Waite, J. N. Israelachvili, The contribution of DOPA to substrate-peptide adhesion and internal cohesion of mussel-inspired synthetic peptide films. *Adv. Funct. Mater.* **20**, 4196–4205 (2010).
21. H. Lee, N. F. Scherer, P. B. Messersmith, Single-molecule mechanics of mussel adhesion. *Proc. Natl. Acad. Sci. U.S.A.* **103**, 12999–13003 (2006).
22. M. Shin, J. Y. Shin, K. Kim, B. Yang, J. W. Han, N.-K. Kim, H. J. Cha, The position of lysine controls the catechol-mediated surface adhesion and cohesion in underwater mussel adhesion. *J. Colloid Interface Sci.* **563**, 168–176 (2020).
23. K. El Adraa, V. Timon, J.-F. Lambert, A.-R. Al-Rabaa, F. Jaber, M. Jaber, F. Tielens, Adsorption of L-DOPA intercalated in hydrated Na-Saponite clay: A combined experimental and theoretical study. *J. Phys. Chem. C* **116**, 26414–26421 (2012).
24. H. Zhao, N. B. Robertson, S. A. Jewhurst, J. H. Waite, Probing the adhesive footprints of *Mytilus californianus* byssus. *J. Biol. Chem.* **281**, 11090–11096 (2006).
25. J. H. Waite, X. Qin, Polyphosphoprotein from the adhesive pads of *Mytilus edulis*. *Biochemistry* **40**, 2887–2893 (2001).
26. G. P. Maier, M. V. Rapp, J. H. Waite, J. N. Israelachvili, A. Butler, Adaptive synergy between catechol and lysine promotes wet adhesion by surface salt displacement. *Science* **349**, 628–632 (2015).
27. B. K. Ahn, S. Das, R. Linstadt, Y. Kaufman, N. R. Martinez-Rodriguez, R. Mirshafian, E. Kesselman, Y. Talmon, B. H. Lipshutz, J. N. Israelachvili, J. H. Waite, High-performance mussel-inspired adhesives of reduced complexity. *Nat. Commun.* **6**, 8663 (2015).
28. R. Wang, J. Li, W. Chen, T. Xu, S. Yun, Z. Xu, Z. Xu, T. Sato, B. Chi, H. Xu, A biomimetic mussel-inspired ε-poly-L-lysine hydrogel with robust tissue-anchor and anti-infection capacity. *Adv. Funct. Mater.* **27**, 1604894 (2017).
29. Y. Li, C. Liang, L. Gao, S. Li, Y. Zhang, J. Zhang, Y. Cao, Hidden complexity of synergistic roles of Dopa and lysine for strong wet adhesion. *Mater. Chem. Front.* **1**, 2664–2668 (2017).
30. Z. A. Levine, M. V. Rapp, W. Wei, R. G. Mullen, C. Wu, G. H. Zerze, J. Mittal, J. H. Waite, J. N. Israelachvili, J.-E. Shea, Surface force measurements and simulations of mussel-derived peptide adhesives on wet organic surfaces. *Proc. Natl. Acad. Sci. U.S.A.* **113**, 4332–4337 (2016).
31. M. A. Gebbie, W. Wei, A. M. Schrader, T. R. Cristiani, H. A. Dobbs, M. Idso, B. F. Chmelka, J. H. Waite, J. N. Israelachvili, Tuning underwater adhesion with cation–π interactions. *Nat. Chem.* **9**, 473–479 (2017).
32. S. Kim, A. Faghihnejad, Y. Lee, Y. Jho, H. Zeng, D. S. Hwang, Cation–π interaction in DOPA-deficient mussel adhesive protein mfp-1. *J. Mater. Chem. B* **3**, 738–743 (2015).
33. R. Santonocito, F. Venturella, F. Dal Piaz, M. A. Morando, A. Provenzano, E. Rao, M. A. Costa, D. Bulone, P. L. San Biagio, D. Giacomazza, A. Sicorello, C. Alfano, R. Passantino, A. Pastore, Recombinant mussel protein Pvfp-5β: A potential tissue bioadhesive. *J. Biol. Chem.* **294**, 12826–12835 (2019).

34. P. Bilotto, C. Labate, M. P. De Santo, K. Deepankumar, A. Miserez, B. Zappone, Adhesive properties of adsorbed layers of two recombinant mussel foot proteins with different levels of DOPA and tyrosine. *Langmuir* **35**, 15481–15490 (2019).
35. H. J. Cha, D. S. Hwang, S. Lim, J. D. White, C. A. Matos-Perez, J. J. Wilker, Bulk adhesive strength of recombinant hybrid mussel adhesive protein. *Biofouling* **25**, 99–107 (2009).
36. B. K. Ahn, Perspectives on mussel-inspired wet adhesion. *J. Am. Chem. Soc.* **139**, 10166–10171 (2017).
37. W. Wei, J. Yu, M. A. Gebbie, Y. Tan, N. R. Martinez Rodriguez, J. N. Israelachvili, J. H. Waite, Bridging adhesion of mussel-inspired peptides: Role of charge, chain length, and surface type. *Langmuir* **31**, 1105–1112 (2015).
38. B. P. Lee, S. Konst, Novel hydrogel actuator inspired by reversible mussel adhesive protein chemistry. *Adv. Mater.* **26**, 3415–3419 (2014).
39. H. Heinz, B. L. Farmer, R. B. Pandey, J. M. Slocik, S. S. Patnaik, R. Pachter, R. R. Naik, Nature of molecular interactions of peptides with gold, palladium, and Pd–Au bimetal surfaces in aqueous solution. *J. Am. Chem. Soc.* **131**, 9704–9714 (2009).
40. H. Kang, F. X. Vázquez, L. Zhang, P. Das, L. Toledo-Sherman, B. Luan, M. Levitt, R. Zhou, Emerging β-sheet rich conformations in supercompact huntingtin exon-1 mutant structures. *J. Am. Chem. Soc.* **139**, 8820–8827 (2017).
41. D.-A. Silva, D. R. Weiss, F. Pardo Avila, L.-T. Da, M. Levitt, D. Wang, X. Huang, Millisecond dynamics of RNA polymerase II translocation at atomic resolution. *Proc. Natl. Acad. Sci. U.S.A.* **111**, 7665–7670 (2014).
42. L. Petrone, A. Kumar, C. N. Sutanto, N. J. Patil, S. Kannan, A. Palaniappan, S. Amini, B. Zappone, C. Verma, A. Miserez, Mussel adhesion is dictated by time-regulated secretion and molecular conformation of mussel adhesive proteins. *Nat. Commun.* **6**, 8737 (2015).
43. Z. Qin, M. J. Buehler, Molecular mechanics of mussel adhesion proteins. *J. Mech. Phys. Solids* **62**, 19–30 (2014).
44. X. Daura, K. Gademann, B. Jaun, D. Seebach, W. F. van Gunsteren, A. E. Mark, Peptide folding: When simulation meets experiment. *Angew. Chem. Int. Ed.* **38**, 236–240 (1999).
45. D. Ringe, G. A. Petsko, Mapping protein dynamics by x-ray diffraction. *Prog. Biophys. Mol. Biol.* **45**, 197–235 (1985).
46. J. A. McCammon, P. G. Wolynes, M. Karplus, Picosecond dynamics of tyrosine side chains in proteins. *Biochemistry* **18**, 927–942 (1979).
47. M. Karplus, Dynamics of proteins. *Adv. Biophys.* **18**, 165–190 (1984).
48. O. Mancini, O. J. Rolinski, K. Kubiak-Ossowska, P. A. Mulheran, Tyrosine rotamer states in β amyloid: Signatures of aggregation and fibrillation. *ACS Omega* **3**, 16046–16056 (2018).
49. M. R. de Planque, B. B. Bonev, J. A. Demmers, D. V. Greathouse, R. E. Koeppe II, F. Separovic, A. Watts, J. A. Killian, Interfacial anchor properties of tryptophan residues in transmembrane peptides can dominate over hydrophobic matching effects in peptide–lipid interactions. *Biochemistry* **42**, 5341–5348 (2003).
50. H. J. Dyson, P. E. Wright, H. A. Scheraga, The role of hydrophobic interactions in initiation and propagation of protein folding. *Proc. Natl. Acad. Sci. U.S.A.* **103**, 13057–13061 (2006).
51. F. N. Petersen, M. Ø. Jensen, C. H. Nielsen, Interfacial tryptophan residues: A role for the cation–π effect? *Biophys. J.* **89**, 3985–3996 (2005).
52. M. S. Marshall, R. P. Steele, K. S. Thanthiriwatte, C. D. Sherrill, Potential energy curves for cation–π interactions: Off-axis configurations are also attractive. *J. Phys. Chem. B* **113**, 13628–13632 (2009).
53. S. Hong, Y. Wang, S. Y. Park, H. Lee, Progressive fuzzy cation–π assembly of biological catecholamines. *Sci. Adv.* **4**, eaat7457 (2018).
54. P. B. Crowley, A. Golovin, Cation–π interactions in protein–protein interfaces. *Proteins* **59**, 231–239 (2005).
55. E. A. Meyer, R. K. Castellano, F. Diederich, Interactions with aromatic rings in chemical and biological recognition. *Angew. Chem. Int. Ed.* **42**, 1210–1250 (2003).
56. W. Zhong, J. P. Gallivan, Y. Zhang, L. Li, H. A. Lester, D. A. Dougherty, From ab initio quantum mechanics to molecular neurobiology: A cation–π binding site in the nicotinic receptor. *Proc. Natl. Acad. Sci. U.S.A.* **95**, 12088–12093 (1998).
57. S. Kim, H. Y. Yoo, J. Huang, Y. Lee, S. Park, Y. Park, S. Jin, Y. M. Jung, H. Zeng, D. S. Hwang, Y. Jho, Salt triggers the simple coacervation of an underwater adhesive when cations meet aromatic π electrons in seawater. *ACS Nano* **11**, 6764–6772 (2017).
58. I.-C. Yeh, J. L. Lenhart, B. C. Rinderspacher, Molecular dynamics simulations of adsorption of catechol and related phenolic compounds to alumina surfaces. *J. Phys. Chem. C* **119**, 7721–7731 (2015).
59. J. Martí, J. Sala, E. Guàrdia, Molecular dynamics simulations of water confined in graphene nanochannels: From ambient to supercritical environments. *J. Mol. Liq.* **153**, 72–78 (2010).
60. J. Li, T. Liu, X. Li, L. Ye, H. Chen, H. Fang, Z. Wu, R. Zhou, Hydration and dewetting near graphite–CH_3 and graphite–COOH plates. *J. Phys. Chem. B* **109**, 13639–13648 (2005).
61. C.-Y. Gao, Y.-Y. Guo, J. He, M. Wu, Y. Liu, Z.-L. Chen, W.-S. Cai, Y.-L. Yang, C. Wang, X.-Z. Feng, L-3,4-Dihydroxyphenylalanine-collagen modified PDMS surface for controlled cell culture. *J. Mater. Chem.* **22**, 10763–10770 (2012).
62. H. Hu, J. C. Dyke, B. A. Bowman, C.-C. Ko, W. You, Investigation of dopamine analogues: Synthesis, mechanistic understanding, and structure–property relationship. *Langmuir* **32**, 9873–9882 (2016).
63. H. Cheng, K. Yue, M. Kazemzadeh-Narbat, Y. Liu, A. Khalilpour, B. Li, Y. S. Zhang, N. Annabi, A. Khademhosseini, Mussel-inspired multifunctional hydrogel coating for prevention of infections and enhanced osteogenesis. *ACS Appl. Mater. Interfaces* **9**, 11428–11439 (2017).
64. Y. Fu, P. Ren, F. Wang, M. Liang, W. Hu, N. Zhou, Z. Lu, T. Zhang, Mussel-inspired hybrid network hydrogel for continuous adhesion in water. *J. Mater. Chem. B* **8**, 2148–2154 (2020).
65. Y. Zhang, B. Ren, S. Xie, Y. Cai, T. Wang, Z. Feng, J. Tang, Q. Chen, J. Xu, L. Xu, J. Zheng, Multiple physical cross-linker strategy to achieve mechanically tough and reversible properties of double-network hydrogels in bulk and on surfaces. *ACS Appl. Polym. Mater.* **1**, 701–713 (2019).
66. J. R. Burkett, J. L. Wojtas, J. L. Cloud, J. J. Wilker, A method for measuring the adhesion strength of marine mussels. *J. Adhes.* **85**, 601–615 (2009).
67. H. Fan, J. Wang, Z. Tao, J. Huang, P. Rao, T. Kurokawa, J. P. Gong, Adjacent cationic–aromatic sequences yield strong electrostatic adhesion of hydrogels in seawater. *Nat. Commun.* **10**, 5127 (2019).
68. R. Wang, B. Zhou, W. Liu, X.-h. Feng, S. Li, D.-f. Yu, J.-c. Chang, B. Chi, H. Xu, Fast in situ generated ε-polylysine-poly (ethylene glycol) hydrogels as tissue adhesives and hemostatic materials using an enzyme-catalyzed method. *J. Biomater. Appl.* **29**, 1167–1179 (2015).
69. T. Schürpf, Q. Chen, J.-H. Liu, R. Wang, T. A. Springer, J.-H. Wang, The RGD finger of Del-1 is a unique structural feature critical for integrin binding. *FASEB J.* **26**, 3412–3420 (2012).
70. A. Šali, T. L. Blundell, Comparative protein modelling by satisfaction of spatial restraints. *J. Mol. Biol.* **234**, 779–815 (1993).
71. M.-Y. Shen, A. Sali, Statistical potential for assessment and prediction of protein structures. *Protein Sci.* **15**, 2507–2524 (2006).
72. Y. Sugita, Y. Okamoto, Replica-exchange molecular dynamics method for protein folding. *Chem. Phys. Lett.* **314**, 141–151 (1999).
73. A. Patriksson, D. van der Spoel, A temperature predictor for parallel tempering simulations. *Phys. Chem. Chem. Phys.* **10**, 2073–2077 (2008).
74. M. L. Schlegel, K. L. Nagy, P. Fenter, L. Cheng, N. C. Sturchio, S. D. Jacobsen, Cation sorption on the muscovite (001) surface in chloride solutions using high-resolution x-ray reflectivity. *Geochim. Cosmochim. Acta* **70**, 3549–3565 (2006).
75. W. Loewenstein, The distribution of aluminum in the tetrahedra of silicates and aluminates. *Am. Mineral.* **39**, 92–96 (1954).
76. G. Bussi, D. Donadio, M. Parrinello, Canonical sampling through velocity rescaling. *J. Chem. Phys.* **126**, 014101 (2007).
77. H. J. C. Berendsen, J. P. M. Postma, W. F. van Gunsteren, A. DiNola, J. R. Haak, Molecular dynamics with coupling to an external bath. *J. Chem. Phys.* **81**, 3684–3690 (1984).
78. R. T. Cygan, J.-J. Liang, A. G. Kalinichev, Molecular models of hydroxide, oxyhydroxide, and clay phases and the development of a general force field. *J. Phys. Chem. B* **108**, 1255–1266 (2004).
79. J. Huang, A. D. MacKerell Jr., CHARMM36 all-atom additive protein force field: Validation based on comparison to NMR data. *J. Comput. Chem.* **34**, 2135–2145 (2013).
80. K. Vanommeslaeghe, E. Hatcher, C. Acharya, S. Kundu, S. Zhong, J. Shim, E. Darian, O. Guvench, P. Lopes, I. Vorobyov, A. D. Mackerell Jr., CHARMM general force field: A force field for drug-like molecules compatible with the CHARMM all-atom additive biological force fields. *J. Comput. Chem.* **31**, 671–690 (2010).
81. K. Vanommeslaeghe, A. D. MacKerell Jr., Automation of the CHARMM general force field (CGenFF) I: Bond perception and atom typing. *J. Chem. Inf. Model.* **52**, 3144–3154 (2012).
82. W. L. Jorgensen, J. Chandrasekhar, J. D. Madura, R. W. Impey, M. L. Klein, Comparison of simple potential functions for simulating liquid water. *J. Chem. Phys.* **79**, 926–935 (1983).
83. E. A. Dolan, R. M. Venable, R. W. Pastor, B. R. Brooks, Simulations of membranes and other interfacial systems using $P2_1$ and Pc periodic boundary conditions. *Biophys. J.* **82**, 2317–2325 (2002).
84. T. Darden, D. York, L. Pedersen, Particle mesh Ewald: An *N* log(*N*) method for Ewald sums in large systems. *J. Chem. Phys.* **98**, 10089–10092 (1993).
85. B. Hess, H. Bekker, H. J. C. Berendsen, J. G. E. M. Fraaije, LINCS: A linear constraint solver for molecular simulations. *J. Comput. Chem.* **18**, 1463–1472 (1997).
86. B. Hess, C. Kutzner, D. van der Spoel, E. Lindahl, GROMACS 4: Algorithms for highly efficient, load-balanced, and scalable molecular simulation. *J. Chem. Theory Comput.* **4**, 435–447 (2008).
87. W. Humphrey, A. Dalke, K. Schulten, VMD: Visual molecular dynamics. *J. Mol. Graph.* **14**, 33–38 (1996).

Acknowledgments: We thank R. Zhou, C. Zhou, and J. Wang for helpful discussions. We are also grateful for the computational resources provided by the supercomputer TianHe-1A in Tianjin, China. **Funding:** This work is partially supported by the National Natural Science Foundation of China (11722434 and 11874319 to J.L., 11674153 to Y.C., 11804148 to B.X., and 21904088 to L.Y.), the China Postdoctoral Science Foundation (2018M642401 and 2019T120499 to X.O.), and the National Natural Science Foundation of Jiangsu Province (BK20180320 to B.X.). **Author contributions:** J.L. designed the study. X.O. and J.L. performed MD simulations and analysis. L.Y. collected and analyzed the NMR spectra. B.X. and Y.C. performed the lap shear experiments and data analysis. All authors discussed the results and contributed to the writing of the manuscript. **Competing interests:** The authors declare that they have no competing interests. **Data and materials availability:** All data needed to evaluate the conclusions in the paper are present in the paper and/or the Supplementary Materials. Additional data related to this paper may be requested from the authors.

Submitted 17 March 2020
Accepted 12 August 2020
Published 25 September 2020
10.1126/sciadv.abb7620

Citation: X. Ou, B. Xue, Y. Lao, Y. Wutthinitikornkit, R. Tian, A. Zou, L. Yang, W. Wang, Y. Cao, J. Li, Structure and sequence features of mussel adhesive protein lead to its salt-tolerant adhesion ability. *Sci. Adv.* **6**, eabb7620 (2020).

Science Advances

Structure and sequence features of mussel adhesive protein lead to its salt-tolerant adhesion ability

Xinwen Ou, Bin Xue, Yichong Lao, Yanee Wutthinitikornkit, Ranran Tian, Aodong Zou, Lingyun Yang, Wei Wang, Yi Cao and Jingyuan Li

Sci Adv **6** (39), eabb7620.
DOI: 10.1126/sciadv.abb7620